RSC Advances

This is an *Accepted Manuscript*, which has been through the Royal Society of Chemistry peer review process and has been accepted for publication.

Accepted Manuscripts are published online shortly after acceptance, before technical editing, formatting and proof reading. Using this free service, authors can make their results available to the community, in citable form, before we publish the edited article. This *Accepted Manuscript* will be replaced by the edited, formatted and paginated article as soon as this is available.

You can find more information about *Accepted Manuscripts* in the Information for Authors.

Please note that technical editing may introduce minor changes to the text and/or graphics, which may alter content. The journal's standard Terms & Conditions and the Ethical guidelines still apply. In no event shall the Royal Society of Chemistry be held responsible for any errors or omissions in this *Accepted Manuscript* or any consequences arising from the use of any information it contains.

ROYAL SOCIETY OF CHEMISTRY

www.rsc.org/advances

Atomistic insight into the oxidation of monolayer transition metal dichalcogenides: from structures to electronic properties

Hongsheng Liu, Nannan Han, Jijun Zhao[*]

Key Laboratory of Materials Modification by Laser, Ion and Electron Beams (Dalian University of Technology), Ministry of Education, Dalian 116024, China

ABSTRACT: Monolayer transition metal dichalcogenides (TMDs) stand out in two-dimensional (2D) materials due to their potential applications in future microelectronic and optoelectronic devices. In experiments, field effect transistors (FET) based on MoS_2 monolayer are sensitive to the environmental gases, especially O_2. Thus, the oxidation of monolayer TMDs becomes a critical concern. By first-principles calculations, we reveal that perfect single-layer sheet of TMDs keep intact when exposed in O_2 due to the weak physical adsorption of O_2. However, O_2 can be chemically adsorbed on monolayer TMDs (including MoS_2, $MoSe_2$, $MoTe_2$, WS_2, WSe_2, and WTe_2) with single vacancies of chalcogen, which are the most common defects in realistic TMD materials. The adsorption configurations and dissociation behavior of O_2 molecule at vacancy sites as well as the possible diffusion behavior of oxygen adatom on TMD monolayer surface are explored. Oxidation significantly influences the electronic properties of defective MoS_2 monolayer, while other defective TMD monolayers (especially $MoTe_2$ and WTe_2) suffer less from oxidation. Our theoretical results provide valuable atomistic insight into the oxidation of TMD monolayers and are useful for the future design of TMD-based 2D devices.

RSC Advances Accepted Manuscript

RSC Advances Accepted Manuscript

Introduction

The boom of graphene has initiated tremendous research interests in the other two-dimensional (2D) atomic crystals[1-3]. Among these 2D materials, single-layer and few-layer sheets of transition metal dichalcogenides (TMDs) stand out due to their extraordinary physical properties as well as great potentials in technological applications[4-7]. MoS_2, a typical example of TMDs, forms a hexagonal layered crystal structure with weak interlayer van der Waals (vdW) interactions. Each layer of MoS_2 is composed of one layer of molybdenum atoms sandwiched between two layers of sulfur atoms. The intra-layer bonding is covalent and strong, resulting in absence of dangling bonds at clean MoS_2 surface and thus no intrinsic surface states. Most excitingly, monolayer MoS_2 is a direct gap semiconductor with a quasiparticle band gap of 2.8~2.9 eV[8,9] and an optical gap of 1.8 eV[10], which are important for the applications in microelectronic devices. A monolayer MoS_2 field effect transistor (FET) was constructed by Kis's group[11], which exhibited a reasonable charge carrier mobility (~ 200 $cm^2V^{-1}S^{-1}$) and a room-temperature current on/off ratio of 1×10^8. In addition, 2D TMD materials show great potentials for many other applications, such as phototransistors[12,13], analog small-signal amplifier[14], chemical sensor[15-17], thermoelectric nanodevice[18], ultrasensitive photodetector[19], and solar cell[20].

Compared to the gapless graphene, MoS_2 and other 2D semiconducting TMD sheets have finite gaps (e.g., 2.8~2.9 eV for MoS_2[8,9], 2.31 eV for $MoSe_2$[21], 1.77 eV for $MoTe_2$[21], 2.91 eV for WS_2[21], 2.51 eV for WSe_2[21], 1.79 eV for WTe_2[21]) but lower carrier mobility. Moreover, the performance of MoS_2-based FET can be significantly affected by the environmental gases like oxygen. For instance, Qiu et al. found that bi-layer MoS_2 FET is very sensitive to oxygen and water ambient.[22] Chemisorption of oxygen and water reduced the conductance by up to about

RSC Advances Accepted Manuscript

100 times; but this effect could be reversibly recovered by a simple vacuum annealing at 350 K. Park et al. also explored the influence of oxygen environment on tri-layer MoS_2 FET.[23] The current level of the MoS_2-based FET and the carrier mobility of MoS_2 channel were substantially reduced in the O_2 environment, whereas the current can recover to ~80% of the original level after thermally annealing at 350 K in vacuum. They also revealed that polymethyl methacrylate protective layer coated on MoS_2 can effectively protect the MoS_2 FET from suffering the oxygen disturbance.

Since most applications in microelectronics and optoelectronics require sufficiently high electric conductivity and carrier mobility, the effect of oxygen exposure on the electronic properties of TMD-based devices has become a critical concern for their performance under normal conditions. Recently, Tongay and co-workers pointed out that O_2 molecules are physisorbed on perfect monolayer TMDs and monolayer TMDs with sulfur-vacancies through DFT calculations.[24,25] Here we performed systematical *ab initio* calculations to explore oxidation effect on the electronic properties of MoS_2, $MoSe_2$, $MoTe_2$, WS_2, WSe_2 and WTe_2 single layers. We show that perfect TMD monolayer sheets are inert to oxygen adsorption. However, chemical adsorption and dissociation of O_2 molecule occurs at the vacancy sites of TMD monolayers exothermically. According to the computed band structures, the electronic properties of MoS_2 monolayer with vacancy defects suffers greatly from oxidation, while oxidation effect is relatively less prominent for $MoTe_2$ and WTe_2 sheets. Our theoretical results not only give atomistic insights into the oxidation configuration and electronic properties of TMD monolayers under ambient environments but also provide usefull guidance for the design of future microelectronic and optoelectronic devices.

RSC Advances Accepted Manuscript

Computational methods

All calculations were carried out using the Vienna Ab initio Simulation Package (VASP) based on the density functional theory (DFT).[26] The electron-ion interactions were described by the projector augmented wave (PAW) potentials.[27] To treat the exchange-correlation interaction of electrons, we chose the Perdew-Burke-Ernzerhof (PBE) functional within the generalized-gradient approximation (GGA).[28] A kinetic energy cutoff of 500 eV for the planewave basis and a convergence criterion of 10^{-4} eV for the total energies were carefully tested and adopted for all DFT calculations.

Due to the chemical inertness of perfect MoS_2 surface, oxidation of bulk MoS_2 mainly occurs at the edge-plane surfaces and defect sites on the basal-plane surface.[29-31] Monolayer or few-layer MoS_2 materials fabricated from both micromechanical cleavage and CVD methods always contain some stable defects such as single and double sulfur vacancies, vacancy complexes of one molybdenum and three nearby sulfur, vacancy complexes of molybdenum and three nearby disulfur pairs, and antisite defects by exchanging molybdenum and sulfur atom.[32-35] Among them, sulfur single vacancies are most frequently observed, while other kinds of defects are only occasionally found.[34,35] Moreover, single sulfur vacancy can arise under electron irradiation.[33,36] Therefore, here we only considered oxidation at the single chalcogen vacancy (as the major structural defects) of six semiconducting monolayer TMDs, including MoS_2, $MoSe_2$, $MoTe_2$, WS_2, WSe_2 and WTe_2.

In our simulation models, one chalcogen single vacancy (SV) was created in a (4 × 4) supercell of TMD monolayer, ensuring the distance between two single vacancies larger than 12 Å. Such supercell size corresponds to a vacancy density of 7.1×10^{13} cm^{-2}, comparable to the

RSC Advances Accepted Manuscript

experimental density (in the magnitude of 10^{13} cm^{-2}) in the MoS_2 monolayer from micromechanical cleavage.[34] Our test calculations for bigger (6 × 6) supercells of MoS_2 and WS_2 (corresponding to a SV density of ~3.2 × 10^{13} cm^{-2}) show no significant difference from the results of (4 × 4) supercells. The 2D systems were modeled by a slab model with a vacuum space of more than 12 Å to avoid interactions between adjacent periodic images. During geometry optimization, the spacing of **k** point grids was chosen to be 0.03 $Å^{-1}$ and a convergence criterion of 0.02 eV/Å for force was adopted. In order to obtain more accurate energies and electronic properties, denser **k** point meshes with uniform spacing of 0.015 $Å^{-1}$ were used. Bader analysis[37] was preformed to evaluate the charge transfer between TMD monolayers and O_2 molecule. Spin polarized DFT calculations were carried out for all geometry optimization.

The vacancy formation energy E_f^{SV} is defined as:

$$E_f^{SV} = E_{vac} + \mu_X - E_{TMD}, \quad (1),$$

where E_{vac} and E_{TMD} are the energies of the defective (with vacancy) and pristine supercells, respectively. The chemical potential μ_X of chalcogen is taken as the energy of one chalcogen atom in its solid phase (i.e. orthorhombic sulfur, α-Se and α-Te)[38]. The absorption energy E_{ads} of an oxygen molecule on chalcogen vacancy of TMD monolayer is defined as:

$$E_{ads} = E_{vac} + E_{O2} - E_{oxi}, \quad (2),$$

where E_{oxi} is the energy of the oxidized TMD supercell, E_{O2} is the energy of an isolated O_2 molecule in gas phase.

RSC Advances Accepted Manuscript

Results and discussions

Oxygen adsorption and dissociation

Firstly, all six perfect TMD monolayers were well relaxed along with the lattice constants. The calculated 2D lattice constants are 3.183 Å, 3.318 Å, 3.547 Å, 3.182 Å, 3.317 Å and 3.551 Å for MoS_2, $MoSe_2$, $MoTe_2$, WS_2, WSe_2 and WTe_2 monolayers, in agreement with previous results.[21,39] We started from the perfect monolayers of TMDs and placed an oxygen molecule on the supercell of two representative systems, i.e., MoS_2 and $MoTe_2$. DFT-D2 method[40,41] was used to properly take into account the long-range vdW interactions. After optimization, no chemical bond is ever formed between O_2 and TMD layer, with the nearest distance between O atom and S/Te atom of about 3.4~3.5 Å. The calculated absorption energies of oxygen molecule are 58 meV and 10 meV for MoS_2 and $MoTe_2$ monolayers, respectively. The charge density difference between O_2 and perfect MoS_2 monolayer was also calculated and presented in Figure S1 of the Supporting Information. From the charge density difference, no chemical bond occurs between O_2 and perfect MoS_2 monolayer. Previous DFT calculations showed that O_2 can be physisorbed on the MoS_2 surface with a binding energy of 79 meV,[24] which is slightly larger than the absorption energy in our work. The small difference in the adsorption energy may originate from the different kinetic energy cutoff in DFT calculations. It is known that the gaseous O_2 molecule adopts triplet spin state, which is retained when O_2 molecule is adsorbed on perfect TMD monolayers. Such weak vdW interactions clearly indicate that perfect TMD monolayers cannot be oxidized owing to the chemically inert surface with saturated chalcogen ions. Further calculations of electronic band structures show that weak physical adsorption of O_2 has virtually no influence on the electronic properties of TMD monolayers. Hence, in the following

RSC Advances Accepted Manuscript

discussions we will concentrate on the oxidation effect of defective TMD monolayers with single chalcogen vacancies.

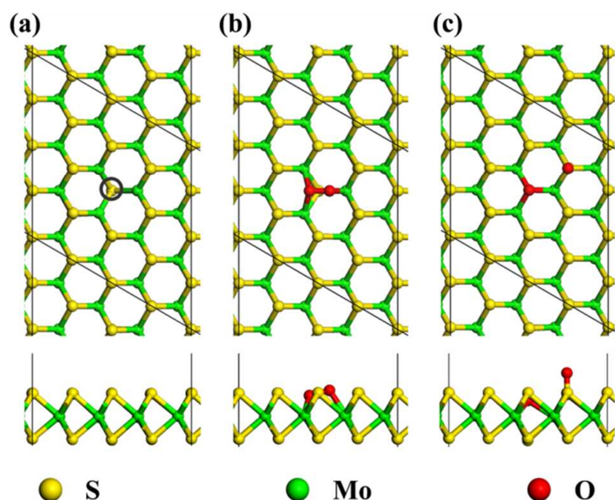

Figure 1. Top views (upper) and side views (lower) of the atomic configurations of (a) MoS_2 monolayer with sulfur SV; (b) MoS_2 monolayer with O_2 molecule adsorption on sulfur SV; (c) oxidized MoS_2 monolayer after O_2 dissociation. Black circle in (a) represents sulfur SV.

For MoS_2, $MoSe_2$, $MoTe_2$, WS_2, WSe_2 and WTe_2, the structures of defective monolayer sheets with single chalcogen vacancy are nearly identical (Figure 1a). Creating a single chalcogen vacancy in the supercell of these TMD sheets does not induce large deformation of the original lattice, that is, the maximum displacement being 0.132 Å and 0.243 Å for chalcogen and metal atoms, respectively. Moreover, our spin polarized calculations show that O_2 molecule adsorbed on the vacancy site of defective TMD monolayers becomes non-magnetic due to formation of TM-O bonds.

RSC Advances Accepted Manuscript

Table 1 lists the formation energies of a chalcogen single vacancy (E_f^{SV}) for all TMD monolayers being explored. For MoX_2 and WX_2 (X=S, Se, Te), the formation energy E_f^{SV} decreases with the increasing of atomic number of chalcogen, which can be understood by the reduction of electronegativity of chalcogen (thus weakening of Mo-X or W-X bond). Among them, WS_2 is most reluctant to form sulfur SV, while creation of sulfur SV is relatively easy from thermodynamic point of view.

Table 1. Formation energy of chalcogen single vacancy E_f^{SV}, adsorption energy E_{ads} and charge transfer (Q) of O_2 molecule on TMD monolayer (positive Q means that O_2 gains electrons).

TMD monolayer	E_f^{SV} (eV)	E_{ads} (eV)	Q (e)
WS_2	2.856	2.082	1.083
WSe_2	2.688	2.433	1.136
WTe_2	2.311	2.805	1.218
MoS_2	2.681	1.843	0.988
$MoSe_2$	2.609	2.155	1.044
$MoTe_2$	2.396	2.537	1.118

For MoS_2, $MoSe_2$, $MoTe_2$, WS_2, WSe_2 and WTe_2 monolayers with SV, the adsorbed O_2 molecule forms covalent bonds with three surrounding TM atoms at the vacancy site, i.e., one O atom with two TM atoms, another O atom with one TM atom (see Figure 1b). The charge

RSC Advances Accepted Manuscript

density difference between O_2 and defective MoS_2 monolayer is shown in Figure S1b of the Supporting Information. Chemical bond between O atoms and Mo atoms and the weakening of O-O bond can be seen, indicating that O_2 adsorbs on defective MoS_2 monolayer chemically. This is quite different from previous DFT results, in which O_2 was predicted to be physisorbed on the sulfur vacancy sites of MoS_2 monolayer[24,25]. As summarized in Table 2, the O-TM bond lengths for all oxidized TMD monolayer sheets are in the range of 2.10~2.12 Å, which are typical covalent bond lengths for transition metal oxides[42]. The O-O bond lengths ($d_{O\text{-}O}$) of O_2 molecules before and after adsorption on TMD monolayers are also presented in Table 2. Compared with the gas-phase molecule, $d_{O\text{-}O}$ in the chemisorbed O_2 is elongated by 0.2~0.3 Å. Such weakening of O-O bond is a natural consequence of formation of O-TM bonds, which are expected to affect the electronic properties of the TMD sheets to certain extent.

Table 2. O-O bond lengths of O_2 molecules in vacuum and chemisorbed on defective TMD monolayers.

	In vacuum	MoS_2	$MoSe_2$	$MoTe_2$	WS_2	WSe_2	WTe_2
$d_{O\text{-}O}$ (Å)	1.23	1.44	1.45	1.48	1.46	1.48	1.53
$d_{O\text{-}TM}$ (Å)	--	2.12 2.06	2.12 2.08	2.12 2.07	2.11 2.05	2.10 2.04	2.10 2.04

The adsorption energies for O_2 on chalcogen vacancies are summarized in Table 1. For all TMD monolayers, the E_{ads} values are positive, indicating that oxidation of defective ultrathin TMD sheets is an exothermic process. Among all these TMD monolayers, the E_{ads} of MoS_2 is smallest, which corresponds to the weakest interaction between O_2 and vacancy. For MoX_2 (X =

RSC Advances Accepted Manuscript

S, Se, Te), the order of E_{ads} is $MoS_2 < MoSe_2 < MoTe_2$. This can be understood by the following picture. In the oxidized MoX_2, O_2 molecule bonds to the unsaturated Mo atoms at the vacancy site and gains electrons from Mo. Specifically, one Mo atom bonds with five X atoms and one O atom. Hence, there is a competition between O and X atoms to gain electrons from the Mo atom. The smaller electronegativity of X atom, the more electrons are transferred from Mo to O and thus the stronger Mo-O bond. Indeed, Bader charge analysis (see Table 1) confirmed this conjecture, i.e., O_2 molecule gains 0.988 electrons from defective MoS_2 sheet, 1.044 electrons from $MoSe_2$, and 1.118 electrons from $MoTe_2$, respectively. The same trend can be also applied to the WX_2 systems. In addition, with the same chalcogen atom (X), O_2 gains more electrons from WX_2 than MoX_2 and interacts more strongly with WX_2 since W has larger reducibility than Mo.

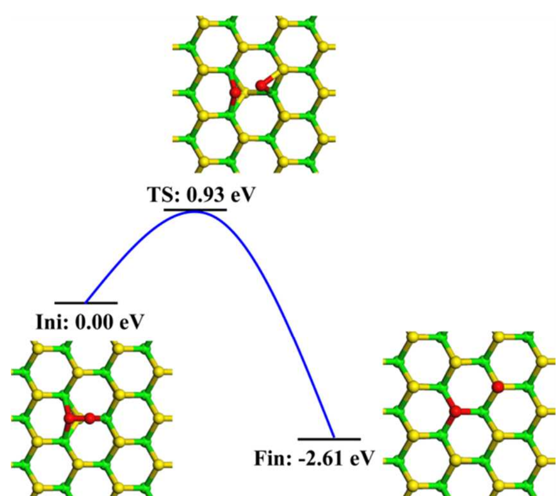

Figure 2. Dissociation process of O_2 on sulfur SV of MoS_2 monolayer.

RSC Advances Accepted Manuscript

To understand the oxidation behavior of defective TMD monolayers, we investigated dissociation of an O_2 molecule at the chalcogen SV with climbing-image nudged elastic band (cNEB) method[43]. For all TMD monolayers considered, the dissociation processes of O_2 molecule at vacancy site remain the same; thus only that for MoS_2 is depicted in Figure 2 as a representative. The structure of oxidized monolayer MoS_2 after O_2 dissociation as the final state is also presented in Figure 1c, in which one oxygen atom at the vacancy site replaces the original missing sulfur and the other one at the top of the adjacent sulfur atom bonds with the sulfur atom perpendicular to the monolayer sheet. Naturally, the two dissociated oxygen atoms at the chalcogen SV are non-magnetic; thus spin polarization was not considered during the transition state search.

The energy barriers and heats of reaction for O_2 dissociation at vacancy site for all the TMD monolayers are summarized in Table 3. For all systems considered, dissociation of oxygen molecule at the chalcogen vacancy is exothermic with heat of reaction ranging from 1.49 eV to 2.61 eV. Oxygen molecule is most reluctant to dissociate at the vacancy of MoS_2 monolayer with an energy barrier of 0.93 eV, while the barrier remains high for WS_2 (0.86 eV) and $MoSe_2$ (0.71 eV). The dissociation barrier reduces to 0.58 eV for WSe_2 and 0.25 eV for $MoTe_2$, whereas there is even no barrier for O_2 dissociation in the case of WTe_2. Therefore, O_2 molecule adsorbed at the chalcogen vacancy sites of the defective $MoTe_2$ and WTe_2 monolayers would easily dissociate into two oxygen atoms at ambient conditions.

RSC Advances Accepted Manuscript

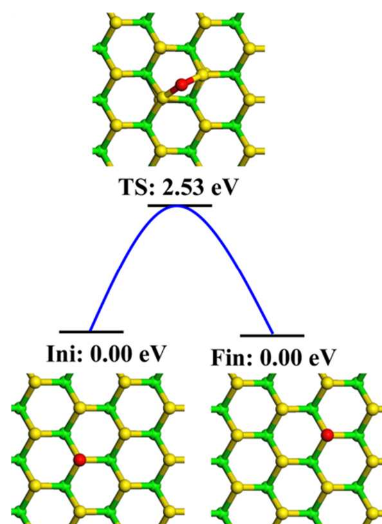

Figure 3. Diffusion behavior of single oxygen atom on perfect MoS_2 monolayer.

After the adsorbed O_2 molecule dissociates on a defective TMD monolayer sheet, one oxygen atom would stay in the original vacancy location and saturate the dangling bond, and another oxygen atom may either stay or migrate to the nearby region of the TMD sheet. The most energetically favorable absorption position for a single oxygen atom on perfect TMD monolayer is the top of chalcogen atom, in accordance with previous studies for oxygen absorbed MoS_2, $MoSe_2$, $MoTe_2$ and WS_2 monolayers[44,45]. To gain further insight into the final structures of oxidized TMD monolayers, we explored the diffusion behavior of an oxygen atom on perfect TMD monolayer. The diffusion path from one top site to another nearby top site is shown in Figure 3, and the corresponding barriers are summarized in Table 3. The barriers for oxygen diffusion on MoS_2 and WS_2 are very high (over 2.5 eV), and it becomes lower on $MoTe_2$ and WTe_2 (around 1.0 eV). Nevertheless, oxygen adatoms are hard to diffuse on TMD monolayers.

RSC Advances Accepted Manuscript

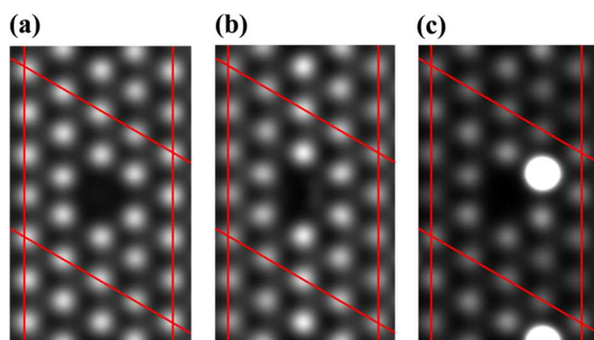

Figure 4. Simulated STM images of (a) TMD monolayers with SV defects with the configuration corresponding to Figure 1a; (b) oxidized MoS_2, $MoSe_2$, WS_2 and WSe_2 monolayers with the configuration corresponding to Figure 1b; (c) oxidized $MoTe_2$ and WTe_2 with the configuration corresponding to Figure 1c.

From the above discussions, we can deduce the most probably atomic structures of oxidized TMD monolayers with vacancy defects. For oxidized MoS_2, $MoSe_2$, WS_2 and WSe_2 monolayers with SV defects, their final structures should correspond to Figure 1b, with oxygen molecules adsorbing on the vacancy sites. For oxidized $MoTe_2$ and WTe_2 monolayers, the most likely structures could be described by Figure 1c, with some oxygen adatom sitting on the top of chalcogen atom and some oxygen adatoms residing at the vacancy site to replace the missing chalcogen atom. To help recognize the configuration of oxidized TMD monolayers in experiments, the STM images of six defective and oxidized TMD monolayers were simulated at bias of −1 V and displayed in Figure 4. In the STM images, each bright point represent a chalcogen atom. As shown in Figure 4a, a SV defect can be clearly seen in the STM image with absence of a bright point in the perfect triangular lattice of bright points, in agreement with previous results.[46] To our surprise, the chemisorbed oxygen molecule cannot be seen in the STM image (Figure 4b), which hints that some other methods should be used to detect the chemisorbed oxygen molecule. After the dissociation of oxygen molecule, a big bright point

RSC Advances Accepted Manuscript

appear in the STM image (Figure 4c) that corresponds to the oxygen adatom at the top of one chalcogen atom, while the other oxygen atom at the vacancy site is still invisible. The different oxidization configurations of defective TMD sheets would lead to different effects on the electronic properties, as we will discuss in the following.

Table 3. Energy barrier (E_a) and heat of reaction (E_{dis}) for dissociation of O_2 on chalcogen SV of TMD monolayer sheets. Energy barrier for diffusion of oxygen atom on perfect TMD monolayers (E_{dif}).

	Oxidized TMD monolayers					
	MoS_2	$MoSe_2$	$MoTe_2$	WS_2	WSe_2	WTe_2
E_a (eV)	0.93	0.71	0.25	0.86	0.58	0.00
E_{dis} (eV)	2.61	1.59	1.54	2.54	1.49	1.49
E_{dif} (eV)	2.53	1.55	0.90	2.68	1.66	1.01

Oxidation effect on electronic band structures

Hereafter we will discuss the electronic properties of six monolayer TMD systems including the perfect sheets, defective sheets and oxidized sheets. Figure 5 displays the band structures of pristine, defective, and oxidized MoX_2 (X = S, Se, Te) monolayers in various circumstances. From our DFT calculations, the perfect MoX_2 monolayer sheets are direct gap semiconductors with band gaps of 1.67 eV, 1.44 eV and 1.09 eV for MoS_2, $MoSe_2$ and $MoTe_2$ respectively (Figure 5a, e, i), in good agreement with previous theoretical values[21,39]. For the defective MoX_2 monolayer, some impurity states in the gap region are induced by chalcogen SV and the top of valence band is substantially disturbed by the SV defect (see Figure 5b, f, g), transforming the defective MoX_2 monolayer sheets into deeply p-type doped semiconductors. The same effect

RSC Advances Accepted Manuscript

was also found in previous DFT calculations.[34,45,46] Interestingly, the SV-induced impurity states in the gap region are completely removed upon adsorption of oxygen molecule (Figure 5c, g, k), simply because of the saturation effect by formation of TM-O bonds at the vacancy sites. However, the valence and conduction bands are still disturbed to certain extent with regard to the pristine MoX_2 monolayers.

RSC Advances Accepted Manuscript

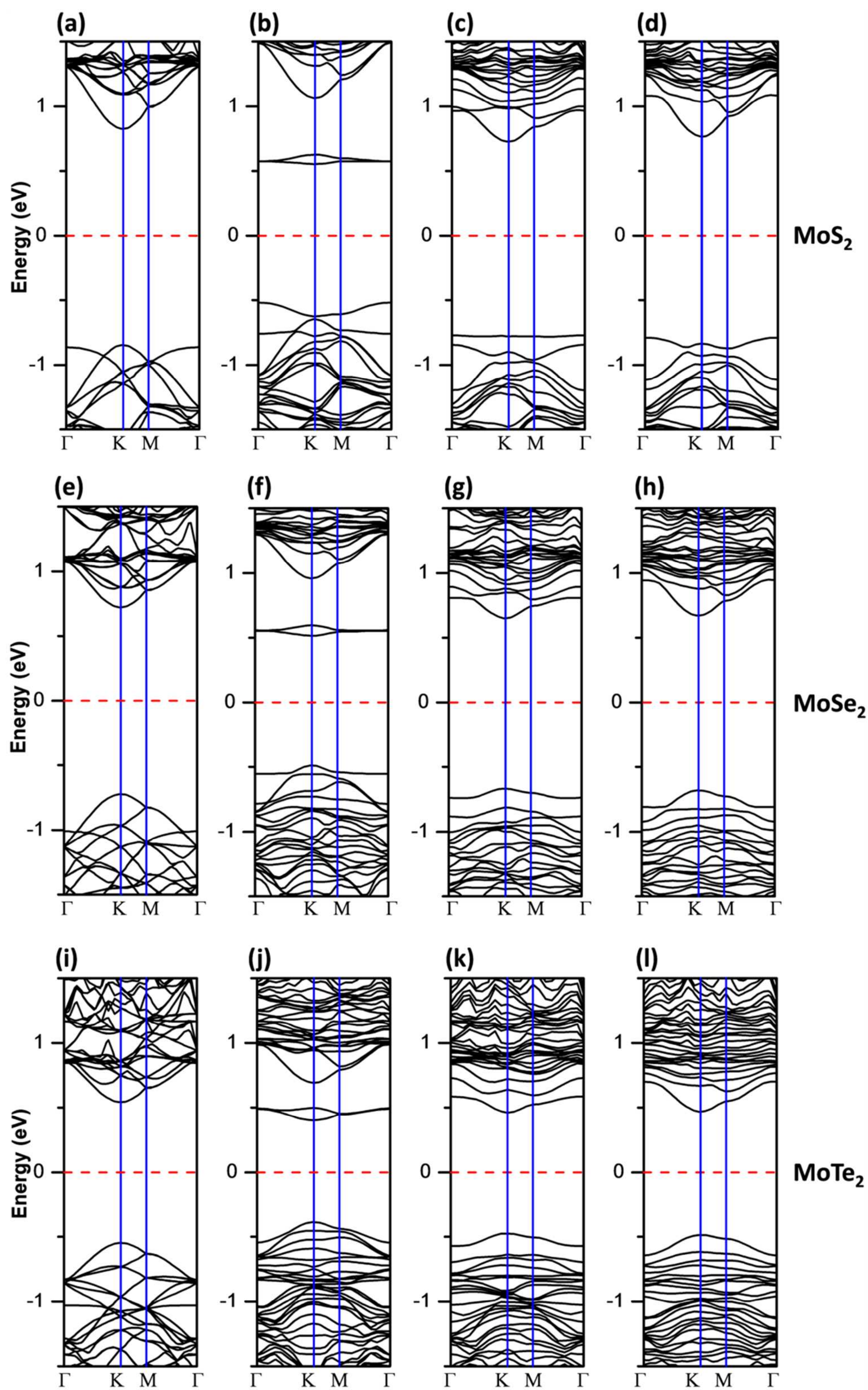

RSC Advances Accepted Manuscript

Figure 5. Band structures of perfect, defective and oxidized MoX_2 monolayer sheets. (a), (e) and (i) present band structures of perfect MoS_2, $MoSe_2$ and $MoTe_2$ monolayer sheets, respectively. (b), (f) and (j) show band structures of MoS_2, $MoSe_2$ and $MoTe_2$ monolayer sheets with chalcogen SV (corresponding to the structure in Figure 1a), respectively. (c), (g) and (k) show band structures of defective MoS_2, $MoSe_2$ and $MoTe_2$ monolayer sheets adsorbed by O_2 molecule (corresponding to the structure in Figure 1b), respectively; (d), (h) and (l) show band structures of defective MoS_2, $MoSe_2$ and $MoTe_2$ monolayer sheets adsorbed with two separated oxygen atoms (corresponding to the structure in Figure 1c). The Fermi level is set to zero (denoted by red dotted line).

After adsorption of oxygen molecule on the defective MoS_2 monolayer, a nearly flat band arises at the top of valence band (Figure 5c), which undoubtedly has a disadvantageous influence on the electronic transport properties. This flat band mainly originates from O_2, since it disappears after dissociation of O_2 at the vacancy site (Figure 5d). A very sharp peak arises at the valence band maximum (VBM) conresponding to the flat band in the partial density of states (PDOS) shown in Figure S2a of the Supporting Information, which confirms that the flat band originates from O_2. Similar to MoS_2, O_2 adsorption on single $MoSe_2$ and $MoTe_2$ layers also induces an isolated band at the top of valence band, but with more pronounced dispersion (Figure 5g, k). In the PDOS of $MoSe_2$ (Figure S2b of the Supporting Information), there is also a sharp peak from O atoms near VBM, but with a small shoulder, which promotes the dispersion of top valance band. For $MoTe_2$, no sharp peak of O atoms arises in the PDOS. (Figure S2c) The different dispersion behaviors of the top valence bands can be related to the interaction strengths between O_2 molecule and TMD sheets. After chemisorption on the TMD layers, the electronic

RSC Advances Accepted Manuscript

level of the O_2 molecule will be broadened due to the formation of O-TM bonds. Intuitively, the stronger O-TM interaction, the broader molecular level of O_2. As presented in Table 1, the interaction between O_2 and vacancy in MoS_2 is weakest among all TMD monolayers explored. Thus, O_2 molecule induces a rather flat band when it is adsorbed at the vacancy site of MoS_2 layer. On the contrary, for $MoSe_2$ and $MoTe_2$, the electronic states of O_2 at the top of valence band are broadened and show certain dispersion due to relatively stronger adsorption interaction.

After the dissociation of O_2 molecule, the features of valence and conduction bands of the oxidized TMD monolayer sheets are partly recovered compared with the perfect monolayers (Figure 5d, h, l). According to above discussions, O_2 molecule is difficult to dissociate at the vacancy sites of MoS_2 and $MoSe_2$ monolayers at ambient conditions. In order to reduce the oxidation effect on the electronic properties of MoS_2 and $MoSe_2$ monolayer sheets, appropriate thermal annealing is needed to promote the dissociation of adsorbed O_2 molecule. In contrast, most O_2 molecules would dissociate on the defective $MoTe_2$ monolayer at room temperature. Therefore, $MoTe_2$ suffers least from oxidation among three MoX_2 monolayers.

RSC Advances Accepted Manuscript

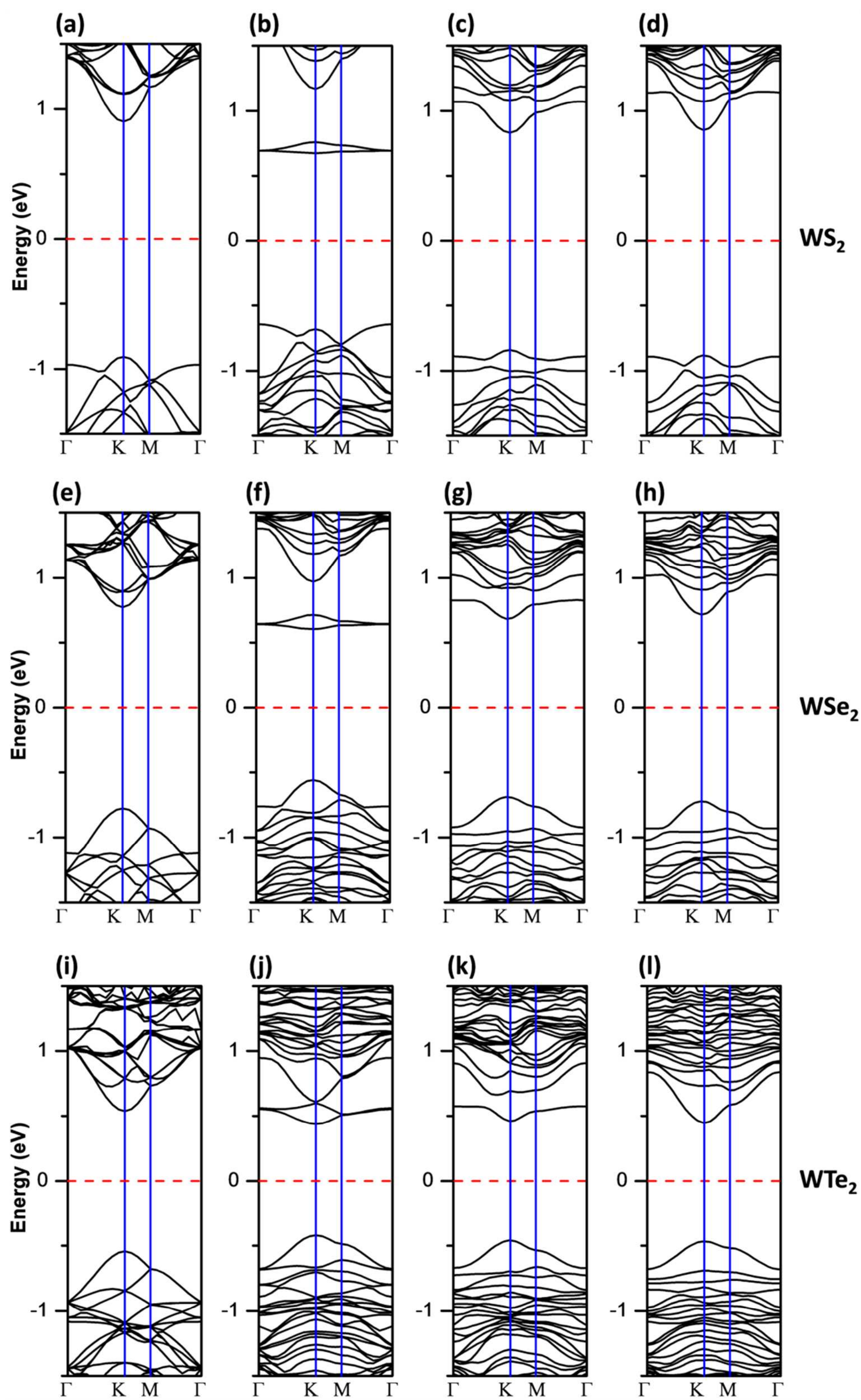

RSC Advances Accepted Manuscript

Figure 6. Band structures of perfect, defective and oxidized WX_2 monolayer sheets. (a), (e) and (i) present band structures of perfect WS_2, WSe_2 and WTe_2 monolayer sheets, respectively. (b), (f) and (j) show band structures of WS_2, WSe_2 and WTe_2 monolayer sheets with chalcogen SV (corresponding to the structure in Figure 1a), respectively; (c), (g) and (k) show band structures of defective WS_2, WSe_2 and WTe_2 monolayer sheets adsorbed by O_2 molecule (corresponding to the structure in Figure 1b), respectively; (d), (h) and (l) show band structures of defective WS_2, WSe_2 and WTe_2 monolayer sheets adsorbed with two separated oxygen atoms (corresponding to the structure in Figure 1c), respectively. The Fermi level is set to zero (denoted by red dotted line).

From our calculations, the perfect WX_2 monolayer sheets are also direct gap semiconductors with band gaps of 1.81 eV (WS_2), 1.55 eV (WSe_2), and 1.08 eV (WTe_2), respectively (Figure 6a, e, i), in accordance with previous theoretical results.[21,39] Similar to the MoX_2 systems, existence of SV defects leads to some impurity states in the gap region (Figure 6b, f, j). However, the valence and conduction bands are less affected by defects; only dispersion of the top valence band is slightly disturbed. When the W atom at chalcogen vacancy is saturated by O_2 adsorption, the impurity states disappear (Figure 6c, g, k). Different from the MoX_2 systems, no sharp peak of O atoms exists in the PDOS of WX_2 (X=S, Se, Te). (Figure S1d, e and f) Thus, no flat band occurs at the top of valence band after O_2 adsorption on the defective WX_2 monolayers. The large dispersion and parabolic shape are well preserved at both the top of valence band and the bottom of conduction band (Figure 6c, g, k). Meanwhile, modification of the conduction bands by O_2 adsorption is more pronounced than that for MoX_2 systems, that is, isolated bands at the bottom of conduction band emerge. After O_2 dissociation, the dispersion of bottom conduction

RSC Advances Accepted Manuscript

band becomes sharp and its shape resemble to that of perfect WX_2 monolayer sheets (Figure 6d, h, l). In other words, O_2 dissociation is indeed helpful to reduce the influence on the electronic properties due to oxidation. Generally speaking, the electronic properties of oxidized WS_2 and WSe_2 sheets should be described by the band structures shown in Figure 6c and Figure 6g respectively, since almost no O_2 molecule is able to dissociate at the vacancy site. On the other hand, all O_2 molecules would dissociate after adsorbing on the defective WTe_2 monolayer. Eventually, oxidation has only little influence on the electronic properties of WTe_2 monolayer, as demonstrated by the band structure shown in Figure 6l.

Table 4. Effective masses of hole and electron carriers (in unit of electron mass m_e) for the perfect TMD monolayers without oxidation and defective TMD monolayers adsorbed by an O_2 molecule or two separated oxygen atoms.

	Perfect sheet		Defective sheet adsorbed with O_2		Defective sheet adsorbed with two O atoms	
	VBM	CBM	VBM	CBM	VBM	CBM
MoS_2	–0.574	0.472	–6.494	0.587	–2.833	0.452
$MoSe_2$	–0.649	0.554	–0.855	0.528	–0.712	0.493
$MoTe_2$	–0.694	0.578	–0.848	0.477	–0.818	0.468
WS_2	–0.410	0.308	–0.535	0.349	–0.457	0.299
WSe_2	–0.439	0.340	–0.516	0.331	–0.498	0.314
WTe_2	–0.417	0.316	–0.509	0.220	–0.527	0.269

RSC Advances Accepted Manuscript

To further understand the oxidation effect on electronic and transport properties of TMD monolayers, we calculated the effective masses of charge carriers at VBM and conduction band minimum (CBM) for the perfect TMD monolayers without oxidation and the defective monolayers with oxidation. The effective mass m^* can be easily derived from band dispersion $E_k(k)$ using the following formula[47]:

$$m^* = \frac{\hbar^2}{d^2E_k(k)/dk^2} \quad (3),$$

where $\hbar$ is the reduced Planck's constant. The theoretical results are summarized in Table 4. First of all, the effective masses of charge carriers for perfect single MoS_2 layer from our band structure calculations coincide well with the previous values (–0.637 m_e for hole and 0.483 m_e for electron).[48]

For the oxidized MoS_2 with O_2 adsorption (corresponding to the structure in Figure 1b), the hole effective mass at VBM is as large as –6.494 m_e, while the increase of electron effective mass at CBM is not prominent compared with the pristine MoS_2 monolayer. Even after O_2 dissociation, the hole effective mass is still very large (–2.833 m_e). In contrast, for oxidized $MoSe_2$ and $MoTe_2$ with O_2 adsorption, the hole effective mass at VBM increases by only about 0.2 m_e and that of electron carrier at CBM even decreases slightly compared with the corresponding perfect monolayers. O_2 dissociation, which easily occurs in oxidized $MoTe_2$ monolayer, weakens the oxidation effect on the effective mass of hole. It is known that the carrier mobility is inversely proportional to its mass.[47] Thus, $MoTe_2$ monolayer suffers least from oxidation among the three MoX_2 monolayers in terms of effective masses and mobilities of carriers.

RSC Advances Accepted Manuscript

As for WS_2 and WSe_2 monolayers, the hole effective mass at VBM increases by about 0.1 m_e and the electron effective mass at CBM only changes slightly upon O_2 adsorption. After the dissociation of O_2, the effective masses of hole and electron of oxidized TMD monolayers are partly recovered. For oxidized WTe_2 monolayer, in which the adsorbed O_2 molecules tend to dissociate at the vacancy sites, the final effective mass of hole (electron) are larger (smaller) than that of perfect sheet by 0.11 m_e (0.047 m_e). The overall carrier mobilities of oxidized WTe_2 layer would be only slightly downgraded with regard to the perfect one.

Implication to device applications

Our theoretical results provide important guidance for the selection of 2D TMD materials for future microelectronic devices. First of all, all perfect TMD monolayers are inert to O_2 molecule, whereas oxidation mainly occurs at the chalcogen single vacancies, which are the most common defects in MoS_2 monolayer materials[34,35]. In order to avoid oxidation and the consequent effects on electronic properties, it is thus desirable to reduce the defect density during the fabrication of TMD sheets. Existence of chalcogen SV induces some impurity states in the gap region and transforms these defective TMD monolayers into deeply p-type doped semiconductors. Interestingly, all SV-induced impurity states in the gap region are completely removed after oxidation, because of the saturation effect by formation of TM-O bonds at the vacancy sites. However, the valence bands and conduction bands are disturbed with regard to the original monolayer sheets to different extents, depending on the specific composition of TMD. The different oxidation effects on the electronic properties of defective TMD monolayers can be related to the interaction strengths between O_2 molecule and the vacancy site of TMD sheets.

RSC Advances Accepted Manuscript

Dissociation of O_2 at the vacancy site further weakens the oxidation effect on electronic properties of TMD monolayers. Fortunately, O_2 can easily dissociate on the oxidized $MoTe_2$ and WTe_2 layers. But dissociation of O_2 is rather difficult in the other four oxidized TMD monolayer sheets due to large energy barrier (0.58~0.93 eV). Among them, MoS_2 monolayer suffers most from oxidation, with a flat band at the top of valence band. In the realistic MoS_2-based devices like FET, a protective layer is usually required.[23] Compared to MoS_2, oxidation effect is less prominent in the WS_2 and WSe_2 monolayer materials. Recently, ambipolar FET based on few-layered WS_2 sheet and p-type FET composed of monolayer WSe_2 sheet have been successfully fabricated in experiments.[49,50] Finally, due to the easy dissociation of O_2, the band structures of $MoTe_2$ and WTe_2 monolayer sheets show some robustness to oxidation. We anticipate $MoTe_2$- or WTe_2- based FET devices to be experimentally fabricated in near future.

Conclusions

Using first-principles calculations, we systematically investigated the oxidation behaviors of several semiconducting TMD monolayers (MoS_2, $MoSe_2$, $MoTe_2$, WS_2, WSe_2 and WTe_2) with single chalcogen vacancies and discussed the oxidation effects on the electronic properties. Without defects, all TMD monolayers are inert to O_2 gaseous molecules; whereas oxidation as an exothermic process mainly occurs at the chalcogen vacancies with adsorption energies of 1.8~3.9 eV. For all semiconducting TMD monolayers explored, chalcogen vacancy can induce some impurity states in the gap region, which can be removed by oxidation. After adsorption, O_2 molecule may further dissociate exothermically by overcoming an energy barrier. Due to small or even zero energy barrier, O_2 molecule would easily dissociate after adsorption on defective

RSC Advances Accepted Manuscript

$MoTe_2$ and WTe_2 monolayers at ambient conditions. For the other four oxidized TMD monolayers, dissociation of O_2 is more difficult. Moreover, it is difficult for oxygen adatoms to diffuse on TMD monolayers because of the large diffusion barriers (0.90~2.68 eV). Simulated STM images indicate that chemisorbed oxygen molecules and oxygen adatoms in the vacancy sites are invisible and that oxygen adatoms on the top of chalcogen atoms result in bright spots in the STM images.

Most importantly, the oxidation effects on the electronic properties of different TMD monolayers are different. Oxidation can badly affect the electronic properties of MoS_2 monolayer. Among MoX_2 and WX_2 systems, $MoTe_2$ and WTe_2 monolayers suffer least from oxidation due to the easy dissociation of O_2, which is helpful to reduce the influence on the electronic properties due to oxidation. No doubt, our results give valuable atomic insight into oxidation of the TMD monolayers. These theoretical findings will not only help understand the oxidation effects on TMD-based 2D materials in current experiments but also provide useful guidance for designing microelectronic devices in the future.

AUTHOR INFORMATION

Corresponding Author

* Corresponding author. E-mail: zhaojj@dlut.edu.cn

ACKNOWLEDGMENT

This work was supported by the National Natural Science Foundation of China (11134005).

RSC Advances Accepted Manuscript

REFERENCES

1. K. S. Novoselov, D. Jiang, F. Schedin, T. J. Booth, V. V. Khotkevich, S. V. Morozov and A. K. Geim. *Proc. Natl. Acad. Sci. U. S. A.* 2005, **102**, 10451-10453

2. J. N. Coleman, M. Lotya, A. O'Neill, S. D. Bergin, P. J. King, U. Khan, K. Young, A. Gaucher, S. De, R. J. Smith, I. V. Shvets, S. K. Arora, G. Stanton, H.-Y. Kim, K. Lee, G. T. Kim, G. S. Duesberg, T. Hallam, J. J. Boland, J. J. Wang, J. F. Donegan, J. C. Grunlan, G. Moriarty, A. Shmeliov, R. J. Nicholls, J. M. Perkins, E. M. Grieveson, K. Theuwissen, D. W. McComb, P. D. Nellist and V. Nicolosi. *Science* 2011, **331**, 568-571

3. M. Xu, T. Liang, M. Shi and H. Chen. *Chem. Rev.* 2013, **113**, 3766-3798

4. Q. H. Wang, K. Kalantar-Zadeh, A. Kis, J. N. Coleman and M. S. Strano. *Nat. Nanotechnol.* 2012, **7**, 699-712

5. M. Chhowalla, H. S. Shin, G. Eda, L.-J. Li, K. P. Loh and H. Zhang. *Nat. Chem.* 2013, **5**, 263-275

6. S. Z. Butler, S. M. Hollen, L. Cao, Y. Cui, J. A. Gupta, H. R. Gutiérrez, T. F. Heinz, S. S. Hong, J. Huang, A. F. Ismach, E. Johnston-Halperin, M. Kuno, V. V. Plashnitsa, R. D. Robinson, R. S. Ruoff, S. Salahuddin, J. Shan, L. Shi, M. G. Spencer, M. Terrones, W. Windl and J. E. Goldberger. *ACS Nano* 2013, **7**, 2898-2926

7. S. Balendhran, S. Walia, H. Nili, J. Z. Ou, S. Zhuiykov, R. B. Kaner, S. Sriram, M. Bhaskaran and K. Kalantar-zadeh. *Adv. Funct. Mater.* 2013, **23**, 3952-3970

8. D. Y. Qiu, F. H. da Jornada and S. G. Louie. *Phys. Rev. Lett.* 2013, **111**, 216805

9. H. Shi, H. Pan, Y.-W. Zhang and B. Yakobson. *Phys. Rev. B* 2013, **87**, 155304

10. K. F. Mak, C. Lee, J. Hone, J. Shan and T. F. Heinz. *Phys. Rev. Lett.* 2010, **105**, 136805

11. RadisavljevicB, RadenovicA, BrivioJ, GiacomettiV and KisA. *Nat. Nanotechnol.* 2011, **6**, 147-150

RSC Advances Accepted Manuscript

12. Z. Yin, H. Li, H. Li, L. Jiang, Y. Shi, Y. Sun, G. Lu, Q. Zhang, X. Chen and H. Zhang. *ACS Nano* 2011, **6**, 74-80

13. H. S. Lee, S. W. Min, Y. G. Chang, M. K. Park, T. Nam, H. Kim, J. H. Kim, S. Ryu and S. Im. *Nano Lett.* 2012, **12**, 3695-3700

14. B. Radisavljevic, M. B. Whitwick and A. Kis. *Appl. Phys. Lett.* 2012, **101**, 043103

15. H. Li, Z. Yin, Q. He, H. Li, X. Huang, G. Lu, D. W. Fam, A. I. Tok, Q. Zhang and H. Zhang. *Small* 2012, **8**, 63-67

16. J. Feng, L. Peng, C. Wu, X. Sun, S. Hu, C. Lin, J. Dai, J. Yang and Y. Xie. *Adv. Mater.* 2012, **24**, 1969-1974

17. F. K. Perkins, A. L. Friedman, E. Cobas, P. M. Campbell, G. G. Jernigan and B. T. Jonker. *Nano Lett.* 2013, **13**, 668-673

18. M. Buscema, M. Barkelid, V. Zwiller, H. S. van der Zant, G. A. Steele and A. Castellanos-Gomez. *Nano Lett.* 2013, **13**, 358-363

19. O. Lopez-Sanchez, D. Lembke, M. Kayci, A. Radenovic and A. Kis. *Nat. Nanotechnol.* 2013, **8**, 497-501

20. M. Bernardi, M. Palummo and J. C. Grossman. *Nano Lett.* 2013, **13**, 3664-3670

21. Y. Ding, Y. Wang, J. Ni, L. Shi, S. Shi and W. Tang. *Physica B: Condensed Matter* 2011, **406**, 2254-2260

22. H. Qiu, L. Pan, Z. Yao, J. Li, Y. Shi and X. Wang. *Appl. Phys. Lett.* 2012, **100**, 123104

23. W. Park, J. Park, J. Jang, H. Lee, H. Jeong, K. Cho, S. Hong and T. Lee. *Nanotechnology* 2013, **24**, 095202

RSC Advances Accepted Manuscript

24. S. Tongay, J. Zhou, C. Ataca, J. Liu, J. S. Kang, T. S. Matthews, L. You, J. Li, J. C. Grossman and J. Wu. *Nano letters* 2013, **13**, 2831-2836

25. S. Tongay, J. Suh, C. Ataca, W. Fan, A. Luce, J. S. Kang, J. Liu, C. Ko, R. Raghunathanan, J. Zhou, F. Ogletree, J. Li, J. C. Grossman and J. Wu. *Sci Rep* 2013, **3**, 2657

26. G. Kresse and J. Furthmüller. *Phys. Rev. B* 1996, **54**, 11169-11186

27. G. Kresse and D. Joubert. *Phys. Rev. B* 1999, **59**, 1758-1775

28. J. P. Perdew, K. Burke and M. Ernzerhof. *Phys. Rev. Lett.* 1996, **77**, 3865-3868

29. S. M. Davis and J. C. Carver. *Applications of Surface Science* 1984, **20**, 193-198

30. W. Jaegermann and D. Schmeisser. *Surf. Sci.* 1986, **165**, 143-160

31. J. Lince and P. Frantz. *Tribol. Lett.* 2001, **9**, 211-218

32. J. S. Ha, H.-S. Roh, S.-J. Park, J.-Y. Yi and E.-H. Lee. *Surf. Sci.* 1994, **315**, 62-68

33. H.-P. Komsa, S. Kurasch, O. Lehtinen, U. Kaiser and A. V. Krasheninnikov. *Phys. Rev. B* 2013, **88**, 035301

34. H. Qiu, T. Xu, Z. Wang, W. Ren, H. Nan, Z. Ni, Q. Chen, S. Yuan, F. Miao, F. Song, G. Long, Y. Shi, L. Sun, J. Wang and X. Wang. *Nat. Commun.* 2013, **4**, 2642

35. W. Zhou, X. Zou, S. Najmaei, Z. Liu, Y. Shi, J. Kong, J. Lou, P. M. Ajayan, B. I. Yakobson and J. C. Idrobo. *Nano Lett.* 2013, **13**, 2615-2622

36. H.-P. Komsa, J. Kotakoski, S. Kurasch, O. Lehtinen, U. Kaiser and A. V. Krasheninnikov. *Phys. Rev. Lett.* 2012, **109**, 035503

37. G. Henkelman, A. Arnaldsson and H. Jónsson. *Comput. Mater. Sci.* 2006, **36**, 354-360

RSC Advances Accepted Manuscript

38. J. Donohue. *The Structures of the Elements*; John Wiley & Sons, Inc. Press: New York, 1974.

39. Q. Yue, Z. Shao, S. Chang and J. Li *Nanoscale Res. Lett.* 2013, **8**, 425

40. S. Grimme. *J. Comput. Chem.* 2006, **27**, 1787-1799

41. T. s. Bučko, J. r. Hafner, S. b. Lebègue and J. n. G. Ángyán. *J. Phys. Chem. A* 2010, **114**, 11814-11824

42. J. B. Parise, E. M. McCarron Iii and A. W. Sleight. *Mater. Res. Bull.* 1987, **22**, 803-811

43. G. Mills, H. Jónsson and G. K. Schenter. *Surf. Sci.* 1995, **324**, 305-337

44. J. He, K. Wu, R. Sa, Q. Li and Y. Wei. *Appl. Phys. Lett.* 2010, **96**, 082504

45. Y. Ma, Y. Dai, M. Guo, C. Niu, J. Lu and B. Huang. *Phys. Chem. Chem. Phys.* 2011, **13**, 15546-15553

46. J. Fuhr, A. Saúl and J. Sofo. *Phys. Rev. Lett.* 2004, **92**, 026802

47. C. Kittel. *Introduction to Solid State Physics*; John Wiley & Sons, Inc. Press: USA, 2005.

48. W. S. Yun, S. W. Han, S. C. Hong, I. G. Kim and J. D. Lee. *Phys. Rev. B* 2012, **85**, 033305

49. D. Braga, I. Gutierrez Lezama, H. Berger and A. F. Morpurgo. *Nano Lett.* 2012, **12**, 5218-5223

50. H. Fang, S. Chuang, T. C. Chang, K. Takei, T. Takahashi and A. Javey. *Nano Lett.* 2012, **12**, 3788-3792

RSC Advances Accepted Manuscript